Synthesis and Characterization of UV-Curable Polyurethane Acrylates Derived from Trimethylolpropane and Hydroxyethyl Methacrylate: Effect of HEMA Content on Thermal Stability, Gloss Properties, and Microstructure

Bilge Eren

bilge.eren@bilecik.edu.tr

Bilecik Universitesi: Bilecik Seyh Edebali Universitesi https://orcid.org/0000-0001-9775-9360

Esra Demir Karaçoban

Bilecik Şeyh Edebali Üniversitesi: Bilecik Seyh Edebali Universitesi

Beyhan Erdoğan

dyo

Research Article

Keywords: Deconvolution analysis, SEM, microstructure, microphase, polyurethane acrylate

Posted Date: January 30th, 2024

DOI: https://doi.org/10.21203/rs.3.rs-3881857/v1

Abstract

This study presents the synthesis of a series of UV-curable polyurethane acrylates (PUAs) derived from trimethylolpropane (TMP) and hydroxyethyl methacrylate (HEMA) through a one-step polymerization method. The phase analysis using FTIR reveals distinct vibration bands corresponding to different functional groups within the polyurethane structure. Thermogravimetric analysis demonstrates two degradation steps in UV-cured $PUA_{3/0}$ films, revealing the influence of HEMA content on thermal stability. Gloss properties exhibit a complex relationship with HEMA content, with initial improvement followed by a decline, emphasizing the impact on film glossiness. Hydrophilic/hydrophobic properties, measured by contact angle values, indicate increased crosslinking and less polar surfaces with higher HEMA content. Microstructure analysis using SEM demonstrates that UV-cured $PUA_{3/0}$ films achieve effective chemical crosslinking and a dense microstructure, contributing to enhanced film properties.

1. Introduction

Polyurethane acrylates (PUAs) synthesized from trimethylolpropane (TMP) constitute a highly versatile polymer class extensively employed across diverse industrial sectors, including coatings, adhesives, and foams [1]. TMP's inclusion in PUAs synthesis is acknowledged for its role in improving mechanical properties and thermal stability in resulting polymers [2]. Various synthesis methods, such as one-step polymerization, prepolymer method, and solution polymerization, can be utilized to produce PUAs based on TMP, influencing properties like composition, molecular weight, and crosslinking density. Adjustments to molecular weight and crosslinking density allow for customization of PUA properties, including glass transition temperature (T_g), with higher crosslinking density corresponding to elevated T_g values [2]. These PUAs are known for their high tensile strength, chemical resistance, and thermal stability.

There is a growing interest in the development of UV-curable Polyurethane Acrylates (PUAs) derived from TMP. These formulations present advantages over traditional systems, such as faster curing times and a diminished environmental impact [3-17]. For instance, Zhu et al.'s research [3] offers valuable insights into manipulating polyurethane composition parameters for controlling particle size, mechanical characteristics, and water resistance in cross-linked waterborne polyurethane films. Wen et al. [4] introduce a novel approach to synthesizing a unique class of PUs with a dual crosslinking network structure achieved through a chemical pre-polymerization process involving TMP, polyethylene glycol, and isophorone diisocyanate. TMP acts as a crosslinker connecting with polyurethane main chains, resulting in a hybrid network structure. Cao et al.'s investigation [5] thoroughly examines the modification of waterborne polyurethane (WPU) films by incorporating TMP, shedding light on film properties and emphasizing critical aspects such as particle size, surface characteristics, gloss, transparency, crosslinking density, tensile properties, and water resistance. The increase in TMP content leads to observable changes in both film structure and performance parameters. To enhance the processing and mechanical properties of PUAs based on TMP, researchers have explored the addition of reactive diluents, such as hydroxyethyl methacrylate (HEMA) [18,19]. In their work, Boton et al. [18] examined the impact of HEMA on the formulation of UV-curable PUA coatings. The study demonstrated enhanced performance

of hyperbranched waterborne PUA coatings in comparison to linear coatings. This enhanced performance was ascribed to the capacity of HEMA to facilitate a greater degree of branching within the polyurethane structure. Similarly, Manvi and Jagtap [19] explored radiation-cured branched polyurethane coatings, highlighting HEMA's significance. HEMA played a dual role, contributing to the structure of branched polyols and imparting distinctive attributes to the coatings. The addition of HEMA enhanced mechanical properties, reduced the T_g, and improved adhesion properties, promoting interfacial bonding with the substrate and accelerating curing.

Fourier-transform infrared (FTIR) spectroscopy is commonly employed to investigate the phase separation characteristics in PUAs. The microphase separation arises when hydrogen bonding is restricted to the hard segment domains, whereas interphase hydrogen bonding facilitates the phase mixing. The distinctions in stretching vibrations observed between hydrogen-bonded amine and free amine, as well as between hydrogen-bonded carbonyl and free amine carbonyl bands, offer valuable insights into the phase characteristics. The analysis of the phase is made by deconvoluting the stretching vibrations of hydrogen-bonded and free C=O as well as N-H groups.

In this study, a series of UV-curable PUAs was synthesized through a one-step polymerization method, using TMP and HEMA. the study aims to provide a comprehensive understanding of the phase behavior, thermal properties, degradation characteristics, glossiness, and microstructure of PUAs, with a focus on the influence of HEMA as a reactive diluent during UV curing. The investigation involved the use of various analytical techniques, such as Fourier Transform Infrared (FTIR) spectroscopy, Differential Scanning Calorimetry (DSC), Thermogravimetric Analysis (TGA), and Scanning Electron Microscopy (SEM). FTIR spectroscopy was employed to elucidate the impact of HEMA capping on the phase behavior between hard and soft segments. This was achieved through the deconvolution analyses of the carbonyl band and free amine band. The formation of hydrogen bonding between urethane N-H and acrylate C=O further contributed to the improved thermomechanical properties. Thermogravimetric analysis (TG/DTG) investigated the thermal degradation of UV-cured PUA films, revealing two distinct degradation steps. While an initial increase in gloss was observed with 40 wt% HEMA, further increases led to a decrease in gloss, attributed to phase separation and agglomeration. The hydrophilic/hydrophobic properties, indicated by contact angle values, demonstrated that a higher HEMA content resulted in increased crosslinking and a more hydrophobic surface. The UV-cured $PUA_{3/0}$ samples exhibited a more uniform and organized crosslinking structure compared to the $PUA_{3/0}$ series, as evidenced by a smoother surface and reduced micropores.

2. Experimental

2.1. Materials

Chemicals from various suppliers were employed in the synthesis of the urethane prepolymer. Specifically, Trimethylolpropane (TMP) was sourced from Fluka, Hexamethylene diisocyanate (HDI) from Sigma-Aldrich, acetone from Merck, and dibutyltin dilaurate (DBTDL) from Sigma-Aldrich. Additionally, 2-

hydroxyethyl methacrylate (HEMA), the acrylate for endcapping, was obtained from Sigma-Aldrich, and the photoinitiator doracure from Fluka. All chemicals were utilized in their original state without undergoing further purification.

2.2. Characterization

EXSTAR SII 7200 thermal analysis instrument was used to study the thermal behaviours of PUAs. The samples were heated in the temperature range of 30°C to 1000°C, with an increase at a heating rate of 10°C/min. The glass transition temperature (T_g) was measured using the PerkinElmer DSC 6000 under a nitrogen atmosphere. The analysis was made in the temperature range of -50°C to 150°C, employing a heating rate of 10°C/min. The investigation of functional groups was conducted using the Perkin–Elmer Spectrum-100 FTIR spectrometer. Gloss measurements of PUA films were recorded at 20°, 60°, and 85° angles using a Byk Micro TRI Gloss. Contact angles were determined using an Attension Theta Lite along with a Hamilton Syringe 1001 TPLT. The ZEISS Supra 40 VP SEM instrument was utilized to examine the surfaces of PUA films.

2.3. Preparation of PUAs

The preparation of PUA oligomers was achieved in a round-bottom flask under a nitrogen atmosphere with stirring. Hexamethylene diisocyanate (HDI) at 0.03 mol equivalent and DBTDL catalyst were introduced, and TMP at 0.01 mol equivalent, diluted with 5 mL of acetone, was added dropwise. This reaction, conducted at approximately 40°C for 3 hours, resulted in the formation of the polyurethane prepolymer. End-capping was achieved by adding 0.03 mol equivalent of HEMA, and the reaction was considered complete when the -NCO peak disappeared entirely from the FT-IR spectra.

2.4. UV curing process

In the formulation of the UV-curable film, a blend of PUA oligomer, Doracure, and HEMA was prepared in a flask. This process took place under a nitrogen atmosphere while employing stirring. The reaction occurred at room temperature for 2 hours. The resultant mixtures were coated onto a transparent polycarbonate sheet to create 50 ± 5 µm thick films. These films were then exposed to a 2-W UVA light source (365 nm) at different curing times for monitoring curing behavior and subsequent characterization. The distance between the sample and the UV light source was maintained at 2 cm.

3. Results ans discussion

3.1. Phase analysis of PUAs using FTIR technique

The PUA exhibits various vibration bands in the IR spectrum, which correspond to different functional groups within the polyurethane structure (Table 1 and Fig. 1). The stretching vibration (v) of the N-H bonds in the urethane groups occurs at 3325 cm^{-1}, while the asymmetric stretching vibrations (va) of the CH2 groups in the aliphatic chains of $PUA_{3/0}$ are observed at 2931 cm^{-1}. The v(C = O) vibration in the amide groups occurs at 1683 cm^{-1}, and the combined vibrations of δ(C-N-H) + v(C-N) in the amide

groups are observed at 1517 cm^{-1}. At 1450 cm^{-1}, the band indicates the CH2 scissoring vibration, and at 1224 cm^{-1}, it corresponds to amide III. The band observed at 1057 cm^{-1} represents the C-O-C stretching vibration of the ester group, while 999 cm^{-1} is indicative of CH2 rocking. Furthermore, the presence of the 878 cm^{-1} band is associated with the C-H bending vibration.

Table 1
FT-IR charecteristic band assigments for PUA synthesis.

Frequency (cm^{-1})	Group	Assignment[a]	In this study
3400–3500	N-H	υ (N-H), free N-H	3484
3310–3350	N-H	υ (N-H), bonded (N-H…O = C)	3334
3260–3300	N-H	υ (N-H), bonded (N-H…O)	-
2890–3050	C-H	$\upsilon_a(CH_2)$	2931
2850–2880	C-H	$\upsilon_s(CH_2)$	2858
2240–2270	N = C = O	υ (NCO)	-
1720–1740	C = O	υ (C = O), free C = O	1724
1700–1715	C = O	υ (C = O), bonded (N-H…O = C), disordered	1712
1670–1685	C = O	free urea	1683
1500–1550	Amide II	δ(C-N-H) + υ (C-N)	1517
1430–1500	C-H	δ (CH_2)	1469
1360–1400	C-H	ω(CH_2)	1306
1220–1230	C-N	urethane	1228
1200–1300	Amide III	δ (N-H) + δ (C-N)	1243
1000–1020	C-H	r (C-H)	1012

[a] υ = stretching, a = asymmetric, s = symmetric, δ = bending, ω = wagging, r = rocking.

The deconvolution of the carbonyl region involved fitting four peaks to elucidate contributions from H-bonded urethane, free urea, mono-dentate H-bonded urea, and bi-dentate H-bonded urea, as illustrated in Fig. 2 and summarized in Table 2. The degree of phase separation in $PUA_{3/0}$ was indicated by the ratio of the absorption bands at 1718 and 1640 cm^{-1}. The former indicated the presence of free urea, while the latter indicated bidentate urea that interacted through hydrogen bonding with surrounding molecules (Scheme 2). The v(C = O) vibration of the monodentate urea groups is at 1683 cm^{-1}, and the v(C = O) vibration of the bidentate urea groups is at 1637 cm^{-1}. Finally, the v(C = O) vibration of the free urethane

groups is at 1715 cm^{-1}. These assignments are based on references [24–25], which reported similar observations in their studies of PUA. The aggregation of hard segments, specifically the urea-urea linkage, can be promoted by bidentate and monodentate H-bonding, leading to microphase separation.

Table 2
Data obtained from deconvolution of N-H bands for PUAs using Gaussian fitting function.

Formulation	C = O							
	Free Ur		H-bonded Ur		Free U		Bidenatate U	
	cm^{-1}	Area	cm^{-1}	Area	cm^{-1}	Area	cm^{-1}	Area
$PUA_{3/0}$	-	-	1712.98	4.5089	1683.50	7.5014	1637.86	3.0337
$UV_{40}PUA_{3/0}$	1724.31	1.5331	1706.76	1.6032	1683.09	5.9446	1636.60	1.7516
$UV_{60}PUA_{3/0}$	1724.12	1.2535	1706.76	1.1751	1683.04	4.4313	1636.52	1.2980
$UV_{80}PUA_{3/0}$	1723.79	1.6464	1706.29	1.6096	1683.09	5.8700	1636.57	1.7142
Ur = Urethane, U = urea.								

The analysis of the FTIR spectra revealed a higher percentage of peak area assigned to H-bonded N–H groups compared to free N–H groups, suggesting a phase-mixed material. This observation is consistent with the presence of interphase H-bonding between the hard and soft segments of the polyurethane. In the N-H region, a change in peak shape was observed following UV-cured PUA. To elucidate this change, three peaks were fitted. The first peak, ranging from 3400 cm^{-1} to 3650 cm^{-1}, was utilized to determine the presence of free amine groups. The second peak, between 3340 cm^{-1} and 3400 cm^{-1}, accounted for the carbonyl overtone, while the third peak, ranging from 3250 cm^{-1} to 3340 cm^{-1}, identified the contribution from H-bonded amine groups. Deconvolution was performed by fitting three bands to the amine region in Fig. 3, aiming to discern the contributions of each type of amine. The summarized data can be found in Table 3. It can be observed that the peak area attributed to the H-bonded amine group is greater than that of the free amine group, which supports the phase-mixed nature of the material. The area of H-bonded amine groups to free amine groups was calculated from the analysis. After UV curing process, the area of H-bonded amine group for $PUA_{3/0}$ decreased from 8.05 for to 7.18, 5.22 and 6.97 for $UV_{40}PUA_{3/0}$, $UV_{60}PUA_{3/0}$, and $UV_{80}PUA_{3/0}$, respectively. As the content of HEMA in the UV cured PUA samples increased, a shift to lower wave numbers was observed in the υ(N–H) region, indicating strong H-bonding interactions. This shift in the maximum amine absorption band to lower frequencies is characteristic of free υ(N–H) and suggests that the presence of HEMA alters the H-bonding interaction in UV cured PUA systems.

Table 3
Data obtained from deconvolution of C = O bands for PUAs using Gaussian fitting function.

Formulation	N-H (Ur + U)					
	Free		C = O Overtone		H-Bonded	
	cm^{-1}	Area	cm^{-1}	Area	cm^{-1}	Area
$PUA_{3/0}$	-	-	-	-	3334.80	8.05
$UV_{40}PUA_{3/0}$	350.44	1.84	3390.62	0.23	3332.18	7.18
$UV_{60}PUA_{3/0}$	3484.39	1.66	3390.72	0.16	3329.80	5.22
$UV_{80}PUA_{3/0}$	3485.71	2.32	3390.82	0.29	3326.82	6.97
Ur = Urethane, U = urea.						

3.2. Thermal behaviors of PUAs

The DSC analysis conducted on both PUA oligomer and its cured films, with varying concentrations of HEMA as the reactive diluent, has provided valuable insights into the impact of the diluent on the material properties. The T_g of the cured films increased with the higher percentage of HEMA in the films (Fig. 4). Specifically, the T_g value of the $PUA_{3/0}$ polymer was determined to be -1.09°C. For films with different concentrations of HEMA (ranging from 40–80 wt %), the T_g value was observed to shift from 35.41 to 48.95°C, respectively (Table 4).

Table 4
DSC data of PUA samples.

Sample	T_g (°C)	ΔC_p (J/(g°C))
$PUA_{3/0}$	-1.09	0.377
$UV_{40}PUA_{3/0}$	35.41	0.320
$UV_{60}PUA_{3/0}$	41.96	0.567
$UV_{80}PUA_{3/0}$	48.95	0.510

The rise in T_g values, corresponding to the increased percentage of HEMA, signifies enhanced cross-linking of the PUA films. This improvement is attributed to the conversion of C = C bonds in the diluent during UV curing. This phenomenon is primarily a result of the higher cross-link density between HEMA and hard segments [26–31]. The formation of hydrogen bonding between the urethane N-H and acrylate C = O in the reactive monomer phase contributes to this effect. Due to its greater compatibility with the hard segments owing to their similar polarity, the reactive monomer phase is believed to establish

stronger bonds and cross-links with the hard segments. The heightened cross-link density restricts the mobility of the polymer chains, leading to enhanced thermomechanical properties in the UV-cured PUAs.

3.3. Thermogravimetric analysis of PUAs

The thermal behavior of UV-cured $PUA_{3/0}$ films was investigated using TG/DTG. Two distinct degradation steps were identified, occurring approximately between 250°C to 400°C and 400°C to 550°C (Fig. 5). Zhao et al. [32] conducted a similar study, revealing a two-step thermal decomposition behavior in all films. Their findings indicated that the thermal degradation process of PUA systems typically initiates with the breakage of urethane bonds, followed by ester bonds in non-isocyanate urethane acrylate systems.

The first step involves the decomposition of urethane and urea bonds in the temperature range of 250°C and 400°C [33]. Urethane linkages decompose within the temperature range of 321°C and 342°C. Throughout this step, the films undergo a weight loss of 20–40%, occurring between 300°C and 385°C. In the second step, occurring between 400°C and 500°C, the main weight loss of 60–90% is observed during the decomposition of isocyanurate and carbodiimide structures (Table 5). When the HEMA content increased from 0–80%, the 5% weight-loss temperature (T5) decreased from 204°C to 178°C.

Table 5
The thermal properties of PUA samples.

Sample	Thermal degradation step	T_{max}/ °C	$(dw/dt)_{max}$ (% min^{-1})	$T_{5\%}$/ °C	$T_{10\%}$/ °C	$T_{30\%}$/ °C	$T_{50\%}$/ °C
$PUA_{3/0}$	I	321	7.36	204	271	324	364
	II	450	11.69				
$UV_{40}PUA_{3/0}$	I	330	7.17	164	210	313	379
	II	452	20.57				
$UV_{60}PUA_{3/0}$	I	339	5.24	191	246	335	408
	II	442	19.59				
$UV_{80}PUA_{3/0}$	I	342	4.14	178	241	329	390
	II	442	15.89				

The decomposition of PUA at 10 wt% took place at 271°C with 0 wt% HEMA content, at 210°C with 40 wt% HEMA, at 246°C with 60 wt% HEMA, and at 241°C with 80 wt% HEMA. To analyze the thermal properties of various UV- $PUA_{3/0}$ films, we measured the maximum thermal degradation temperature (Td) at different mass losses. Td values for UV- $PUA_{3/0}$ films were determined at various mass losses (5%, 10%, 30%, and 50%). The UV40 $PUA_{3/0}$ film displayed Td values of 204°C, 271°C, 324°C, and 370°C at mass losses of 5%, 10%, 30%, and 50%, respectively. Similarly, the UV60 $PUA_{3/0}$ film exhibited T_d values

of 164°C, 210°C, 313°C, and 370°C at the same mass losses, while the UV80 $PUA_{3/0}$ film showed Td values of 191°C, 246°C, 335°C, and 362°C.

PUA systems containing 10 wt% HEMA exhibited degradation at 271°C in the absence of HEMA. However, as the amount of HEMA increased (40 wt%, 60 wt%, and 80 wt%), the temperature at which degradation initiated decreased to 210°C, 246°C, and 241°C, respectively. The presence of HEMA affected the thermal stability of the resulting UV-cured films, with an increase in HEMA content correlating with a decrease in degradation temperature and changes in the shape of weight loss curves. When the crosslink density is low, the hard segments disperse more evenly in the soft segment, resulting in a less ordered structure and lower thermal stability. However, as the crosslink density reaches a certain degree, the hard segments combine more tightly, leading to improved thermal stability. This is attributed to steric hindrance, which limits the ability of the hard segments to move and interact with each other.

3.4. Gloss properties of PUA films

The film cured from the $PUA_{3/0}$ prepolymer exhibited the lowest gloss value compared to other films (refer to Table 6). Initially, the gloss increased with the addition of 40 wt% HEMA, but it decreased with further increases to 60–80 wt%. The initial rise in gloss with 40 wt% HEMA addition may result from the formation of a smoother surface. HEMA enhances polymer chain mobility, improving leveling and reducing surface roughness, thereby enhancing gloss. $PUA_{3/0}$ film gloss values decreased with increasing HEMA content, especially at 60–80 wt%. Excessive dilution can lead to low viscosity, causing phase separation or agglomeration, resulting in surface defects and reduced gloss.

Table 6
Gloss and contact angle measurements of PUA films.

Sample	Gloss (°)			Contact Angle (°)
	20	60	85	
$PUA_{3/0}$	152	155	102	73
$UV_{40}PUA_{3/0}$	163	159	108	73
$UV_{60}PUA_{3/0}$	156	154	105	80
$UV_{80}PUA_{3/0}$	123	145	96	82

Moreover, excessive dilution of the $PUA_{3/0}$ prepolymer may lead to incomplete curing and reduced final product physical properties. For instance, at a 20-degree angle, gloss values for PUAH-3/0 films with varying HEMA ratios were 163, 156, and 123 for UV40 $PUA_{3/0}$, UV60 $PUA_{3/0}$, and UV80 $PUA_{3/0}$ films, respectively. This suggests that as HEMA content increases, film gloss decreases, highlighting the influence of HEMA on film glossiness.

3.5. CA studies of PUA films

The contact angle (CA) value of a PUA prepolymer increases with a higher HEMA content. This observation suggests that the polyurethane film undergoes increased crosslinking, indicating the interconnection of polymer chains into a three-dimensional network. Generally, such a crosslinked network is more stable and less reactive compared to an uncrosslinked polymer, resulting in a less polar surface and a higher contact angle. Therefore, the rise in the CA value with increasing HEMA content can be attributed to changes in the polymer structure and the presence of hydrophobic groups on the surface.

In the case of a PUA prepolymer, the increase in CA value with higher HEMA content can be explained by the diluent effect of HEMA on the polymer structure. HEMA monomers act as spacers between PUA prepolymer chains, causing an expansion in the average distance between the chains. This expanded spacing reduces the density of the polymer network, resulting in a more open and porous structure. Consequently, this more open and porous structure leads to a larger surface area and more available hydrophobic groups on the polymer surface, contributing to an elevated CA value.

3.6. Microstructure analysis of PUA films using SEM technique

SEM images were examined to analyze the fracture surfaces of PUA samples, providing insights into the microstructure of PUA films, as shown in Fig. 6. The surface of the $PUA_{3/0}$ sample (Fig. 6a-c) exhibited roughness characterized by micropores and irregularities, indicating a lower crosslinking density. In contrast, the surface of UV60 $PUA_{3/0}$ (Fig. 6d-f) appeared comparatively homogeneous and smooth, suggesting that the branched structures of HEMA chains contribute to a more uniform and organized crosslinking structure.

The microstructure of UV60$PUA_{3/0}$ samples exhibited increased smoothness in comparison to the $PUA_{3/0}$ series samples. The absence of cavities on the surface at the 20 and 10 nm scale suggests that the UV-cured $PUA_{3/0}$ series samples attained effective chemical crosslinking and a dense microstructure.

4. Conclusions

The effect of HEMA content as the reactive diluent on the film properties of UV-curable PUAs has been investigated in this study. FTIR and deconvolution techniques were employed to examine the H-bonding and microphase separation characteristics of UV-curable PUAs. The ratio of absorption bands at 1718 and 1640 cm^{-1} indicated the degree of phase separation in $PUA_{3/0}$. UV curing led to a decrease in the area of H-bonded amine groups in $PUA_{3/0}$, indicating changes in H-bonding interactions with reactive diluent components. T_g of cured PUA films increases with higher HEMA percentage, indicating enhanced cross-linking. T_g values for PUA films with 40–80 wt% HEMA shift from 35.41 to 48.95°C, demonstrating a direct correlation. Formation of H-bonding between urethane N-H and acrylate C = O contributes to increased cross-link density. Greater compatibility of reactive monomer phase with hard segments results in stronger bonds and cross-links. The study on the thermal behavior of UV-cured $PUA_{3/0}$ films revealed a

two-step decomposition process and provided insights into the specific decomposition steps involving urethane, urea, isocyanurate, and carbodiimide structures.

The introduction of an initial 40 wt% HEMA led to an enhancement in gloss, possibly attributed to the creation of a smoother surface. However, an excessive addition of HEMA resulted in phase separation and surface defects, leading to a decrease in gloss. Specifically, the gloss values of $PUA_{3/0}$ films exhibited a decline with higher HEMA content, especially within the range of 60–80 wt%.

The observed increase in the CA value of the PUA prepolymer with higher HEMA content is attributed to structural changes in the polymer. This increase is linked to enhanced crosslinking, resulting in a more stable and less polar surface. Additionally, the diluent effect of HEMA contributes to an expanded and porous polymer structure, leading to a larger surface area and more available hydrophobic groups.

The microstructure of UV60 $PUA_{3/0}$ sample showed increased smoothness compared to $PUA_{3/0}$ samples. UV60 $PUA_{3/0}$ sample demonstrated effective chemical crosslinking and a dense microstructure.

Declarations

Authors' Contributions

Bilge EREN is tasked with processing experimental data, conducting analysis, drafting the manuscript, and creating figures. Esra DEMİR KARAÇOBAN is responsible for carrying out the experiments. Beyhan ERDOĞAN is responsible for performing polymer characterization.

References

1. Zhao, H., Zhang, W., Yin, X. et al. TMP-based hyperbranched polyurethane elastomer (HBPUE) packaging material applied to anodic bonding. Chem. Pap. 74, 3975–3986 (2020). https://doi.org/10.1007/s11696-020-01190-6
2. I. Polus, Synthesis of polyurethane coating components with IPDI and TMDI, Holz als Roh- und Werkstoff 61 (2003) 238–240, DOI 10.1007/s00107-003-0390-9
3. Zhua, J., Wu, Z., Xiong, D., Pan, L., & Liu, Y. (2019). Preparation and properties of a novel low crystallinity cross-linked network waterborne polyurethane for water-based ink. Progress in Organic Coatings, 133, 161–168.
4. Wen, J., Pan, M., Yuan, J., Wang, J., Zhu, L., Jia, Z., & Song, S. (2020). Facile fabrication of dual-crosslinked single network heterostructural polyurethane hydrogels with superior mechanical and fluorescent performance. Reactive and Functional Polymers, 146, 104433.
5. Cao, X., Ge, X., Chen, H., & Li, W. (2017). Effects of trimethylol propane and AAS salt on properties of waterborne polyurethane with low gloss. Progress in Organic Coatings, 107, 5–13.

6. Jiao, X., Liu, J., Jin, J., Cheng, F., Fan, Y., Zhang, L., Lai, G., Hua, X., & Yang, X. (2021). UV-Cured Transparent Silicone Materials with High Tensile Strength Prepared from Hyperbranched Silicon-Containing Polymers and Polyurethane-Acrylates. ACS Omega, 6, 2890–2898.
7. Arukula, R., Thota, A., Boga, K., Narayan, R., & Rao, C.R.K. (2018). Investigations on anticorrosive, thermal, and mechanical properties of conducting polyurethanes with tetraaniline pendent groups. Polym Adv Technol, 1–12.
8. Boton, L., Puguan, J.M., Latif, M., & Kim, H. (2018). Synthesis and properties of quick-drying UV-curable hyperbranched waterborne polyurethane coating. Progress in Organic Coatings, 125, 201–206.
9. Che, J.-Y., Cheon, J.-M., Chun, J.-H., Park, C.-C., Lee, Y.-H., & Kim, H.-D. (2017). Preparation and properties of emulsifier-/solvent-free slightly crosslinked waterborne polyurethane-acrylic hybrid emulsions for footwear adhesives (III)–effect of trimethylol propane (TMP)/ethylene diamine (EDA) content. Journal of Adhesion Science and Technology, 31(17), 1872-1887.
10. Guo, L., Huang, S., & Qu, J. (2018). Synthesis and properties of high-functionality hydroxyl-terminated polyurethane dispersions. Progress in Organic Coatings, 119, 214–220.
11. Lai, X., Shen, Y., & Wang, L. (2011). Preparation and properties of self-crosslinkable polyurethane/silane hybrid emulsion. J Polym Res, 18, 2425–2433.
12. Park, J.-M., Kim, S.Y., An, S.-K., Lee, Y.-H., & Kim, H.-D. (2017). UV-Curable Fluorinated Crosslinkable Polyurethane-Acrylates for Marine Antifouling Coatings. Clean Technol., 23(2), 148-157.
13. Wang, X., Hu, Y., Song, L., Xing, W., Lu, H., Lv, P., & Jie, G. (2010). Effect of antimony doped tin oxide on behaviors of waterborne polyurethane acrylate nanocomposite coatings. Surface & Coatings Technology, 205, 1864–1869.
14. Yuan, M., Wang, S., Li, G., He, S., Liu, W., Liu, H., Huang, M., & Zhu, C. (2021). UV curable hyperbranched polyester polyurethane acrylate for hydraulic machinery coating. Mater. Res. Express, 8, 035104.
15. Zhang, J., Tu, W., & Dai, Z. (2012). Synthesis and characterization of transparent and high impact resistance polyurethane coatings based on polyester polyols and isocyanate trimers. Progress in Organic Coatings, 75, 579–583.
16. Desai, S., Thakore, I.M., Sarawade, B.D., & Devi, S. (2000). Effect of polyols and diisocyanates on thermo-mechanical and morphological properties of polyurethanes. European Polymer Journal, 36, 711±725.
17. He, Y., Zhang, X., Zhang, X., Huang, H., Chang, J., & Chen, H. (2012). Structural investigations of toluene diisocyanate (TDI) and trimethylolpropane (TMP)-based polyurethane prepolymer. Journal of Industrial and Engineering Chemistry, 18(5), 1620-1627.
18. Boton, L., Puguan, J.M., Latif, M., Kim, H. (2018). Synthesis and properties of quick-drying UV-curable hyperbranched waterborne polyurethane coating. Progress in Organic Coatings, 125, 201–206.
19. Manvi, G.N., Jagtap, R.N. (2013). Radiation cured branched polyurethane for coatings. Pigment & Resin Technology, Volume 42, Number 5, 309–316.

20. Wang, F., Hu, J.Q., Tu, W.P. (2008). Study on microstructure of UV-curable polyurethane acrylate films. Progress in Organic Coatings, 62, 245–250.
21. Mohanty, S.R., Mohanty, S., Nayak, S.K., Samal, S.K. (2021). Synthesis and evaluation of novel acrylic and ester-based polyols for transparent polyurethane coating applications. Materials Today Communications, 27, 102228.
22. Hsieh, K.H., Kuo, C.H., Dai, C.A., Chen, W.C., Peng, T.C., Ho, G.H. (2004). Synthesis and Kinetic Studies of UV-Curable Urethane-Acrylates. Journal of Applied Polymer Science, 91, 3162–3166.
23. Kaewpirom, S., Kunwong, D. (2012). Curing behavior and cured film performance of easy-to-clean UV-curable coatings based on hybrid urethane acrylate oligomers. Journal of Polymer Research, 19, 9995.
24. Zuber, M., Shah, S.A.A., Jamil, T., & Asghar, M.I. (2014). Performance behavior of modified cellulosic fabrics using polyurethane acrylate copolymer. International Journal of Biological Macromolecules, 67, 254–259.
25. Zhang, D., Liu, J., Li, Z., Shen, Y., Wang, P., Wang, D., & Hu, X. (2021). Preparation and properties of UV-curable waterborne silicon-containing polyurethane acrylate emulsion. Progress in Organic Coatings, 160, 106503.
26. Kunwong, D., Sumanochitraporn, N., & Kaewpirom, S. (2011). Curing behavior of a UV-curable coating based on urethane acrylate oligomer: the influence of reactive monomers. Songklanakarin Journal of Science and Technology, 33(2), 201-207. doi: 10.1016/j.sajst.2011.03.011.
27. Hu, Y., Feng, G., Shang, Q., Bo, C., Jia, P., Liu, C., Xu, F., & Zhou, Y. (2019). Bio-based reactive diluent derived from cardanol and its application in polyurethane acrylate (PUA) coatings with high performance. Journal of Coatings Technology Research, 16, 499–509.
28. Choi, W.-C., Lee, W.-K., & Ha, C.-S. (2019). Low-viscosity UV-curable polyurethane acrylates containing dendritic acrylates for coating metal sheets. Journal of Coatings Technology Research, 16(2), 377–385. doi: 10.1007/s11998-018-0024-2.
29. Hu, Y., Liu, C., Shang, Q., & Zhou, Y. (2018). Synthesis and characterization of novel renewable castor oil-based UV-curable polyfunctional polyurethane acrylate. Journal of Coatings Technology Research, 15, 77–85. doi: 10.1007/s11998-017-9948-z.
30. Maurya, S. D., Kurmvanshi, S. K., Mohanty, S., & Nayak, S. K. (2017). A Review on Acrylate-Terminated Urethane Oligomers and Polymers: Synthesis and Applications. Journal Name, Pages 625-656. doi: DOI.
31. Feng, J., & Ye, D. (2019). Self-photoinitiating water-diluted polyurethane acrylates and their UV-curing kinetics. Progress in Organic Coatings, 129, 300–308. doi: 10.1016/j.porgcoat.2019.01.006.
32. Wang, X., Soucek, M. D. "Investigation of non-isocyanate urethane dimethacrylate reactive diluents for UV-curable polyurethane coatings." Progress in Organic Coatings, 76 (2013), 1057–1067.
33. Džunuzović, V., Stefanović, I. S., Džunuzović, E. S., Dapčević, A., Šešlija, S. I., Balanč, B. D., Lama, G. C. "Polyurethane networks based on polycaprolactone and hyperbranched polyester: Structural, thermal, and mechanical investigation." (2019), Progress in Organic Coatings, 137, 105305.

Figures

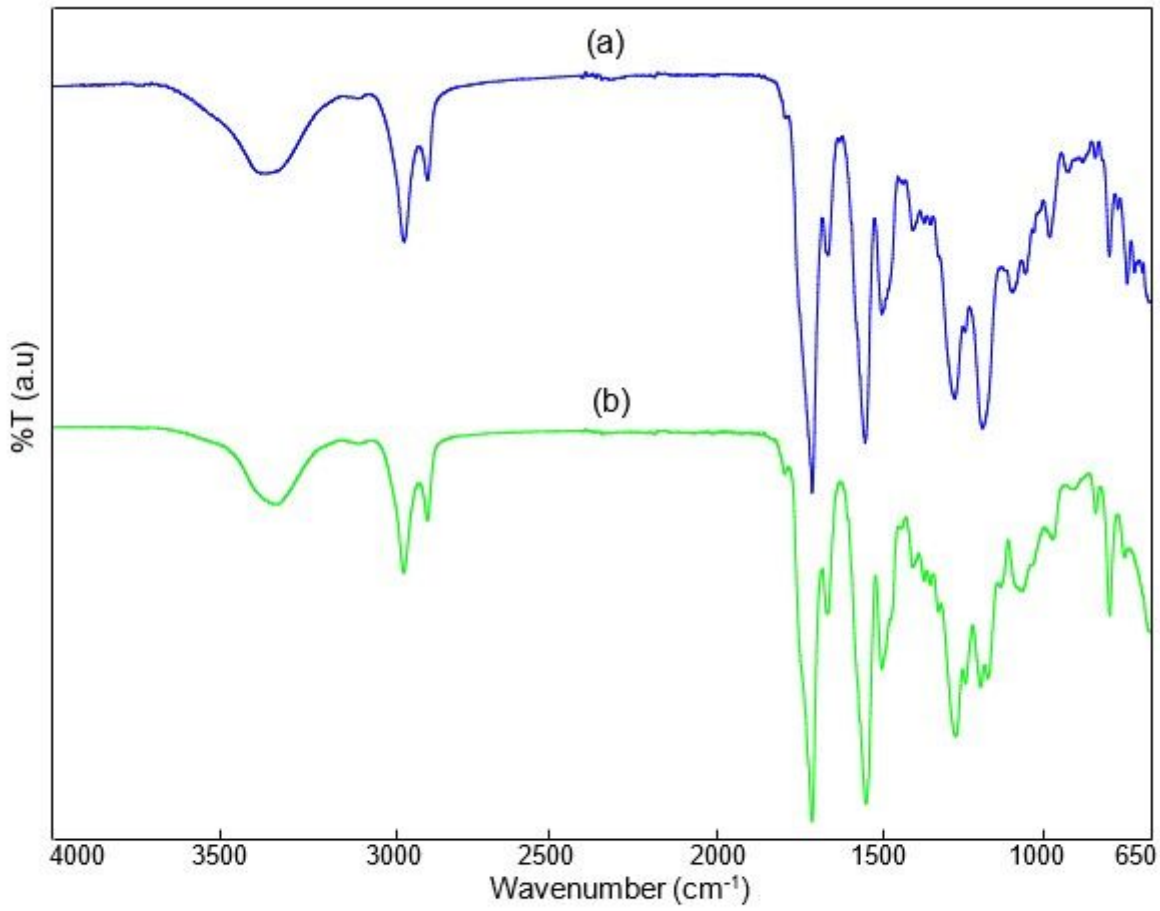

Fig. 1.

Figure 1

FTIR spectra $PUA_{3/0}$ (a), and $UV_{40}PUA_{3/0}$ (b) samples.

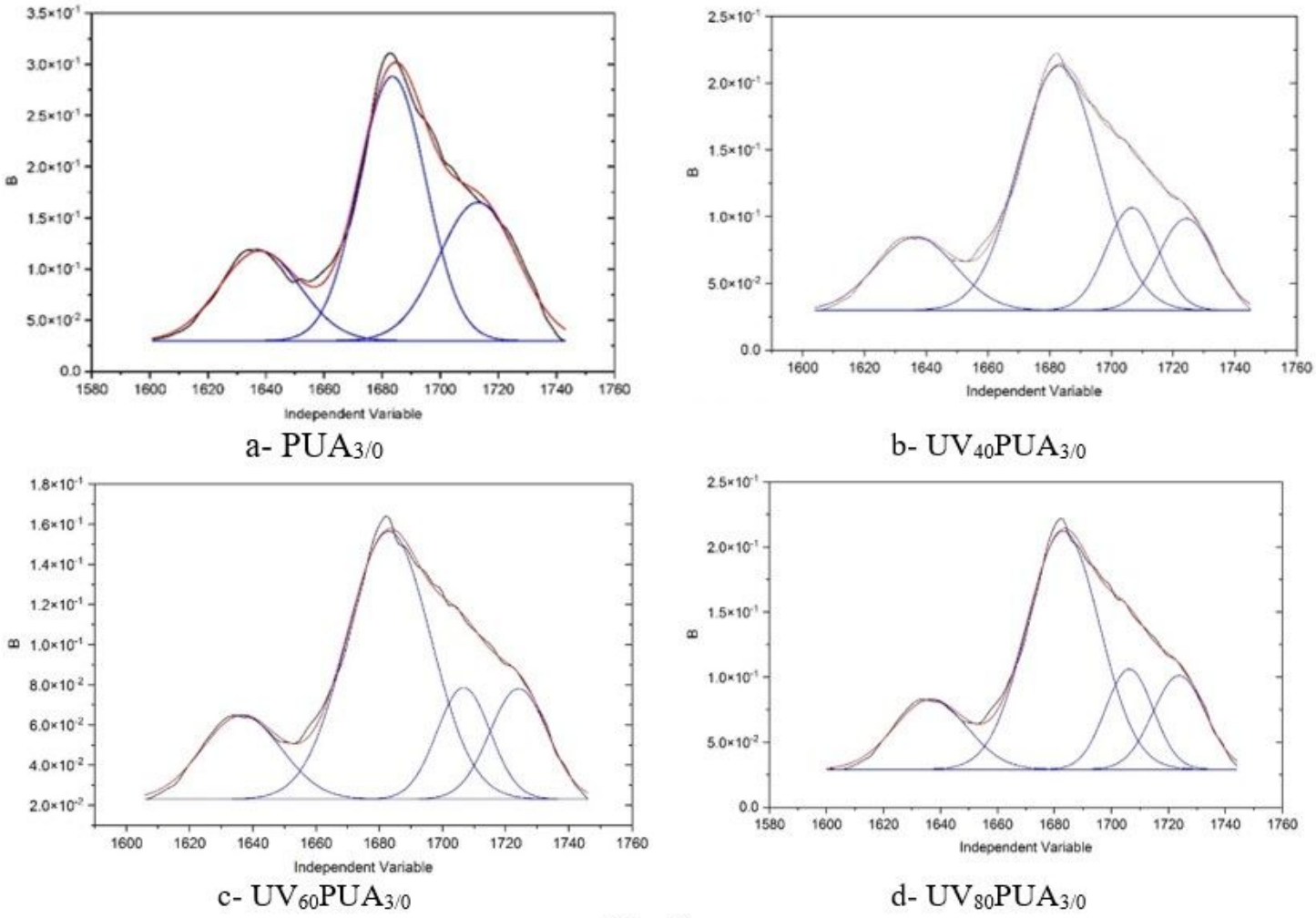

Fig. 2.

Figure 2

Deconvoluted FT-IR spectra of PUAs in the C=O stretching region.

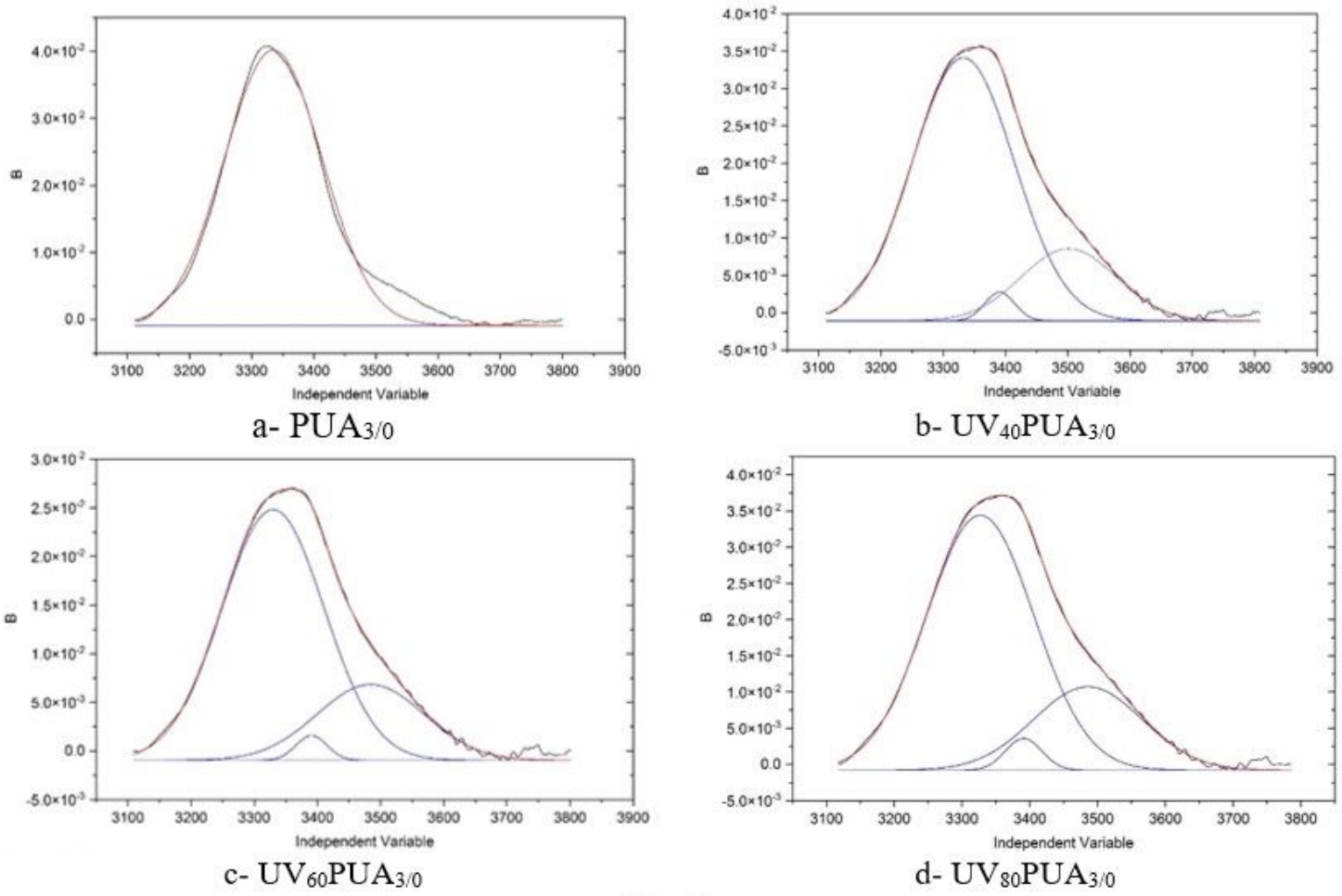

Fig. 3.

Figure 3

Deconvoluted FT-IR spectra of PUAs in the N-H stretching region.

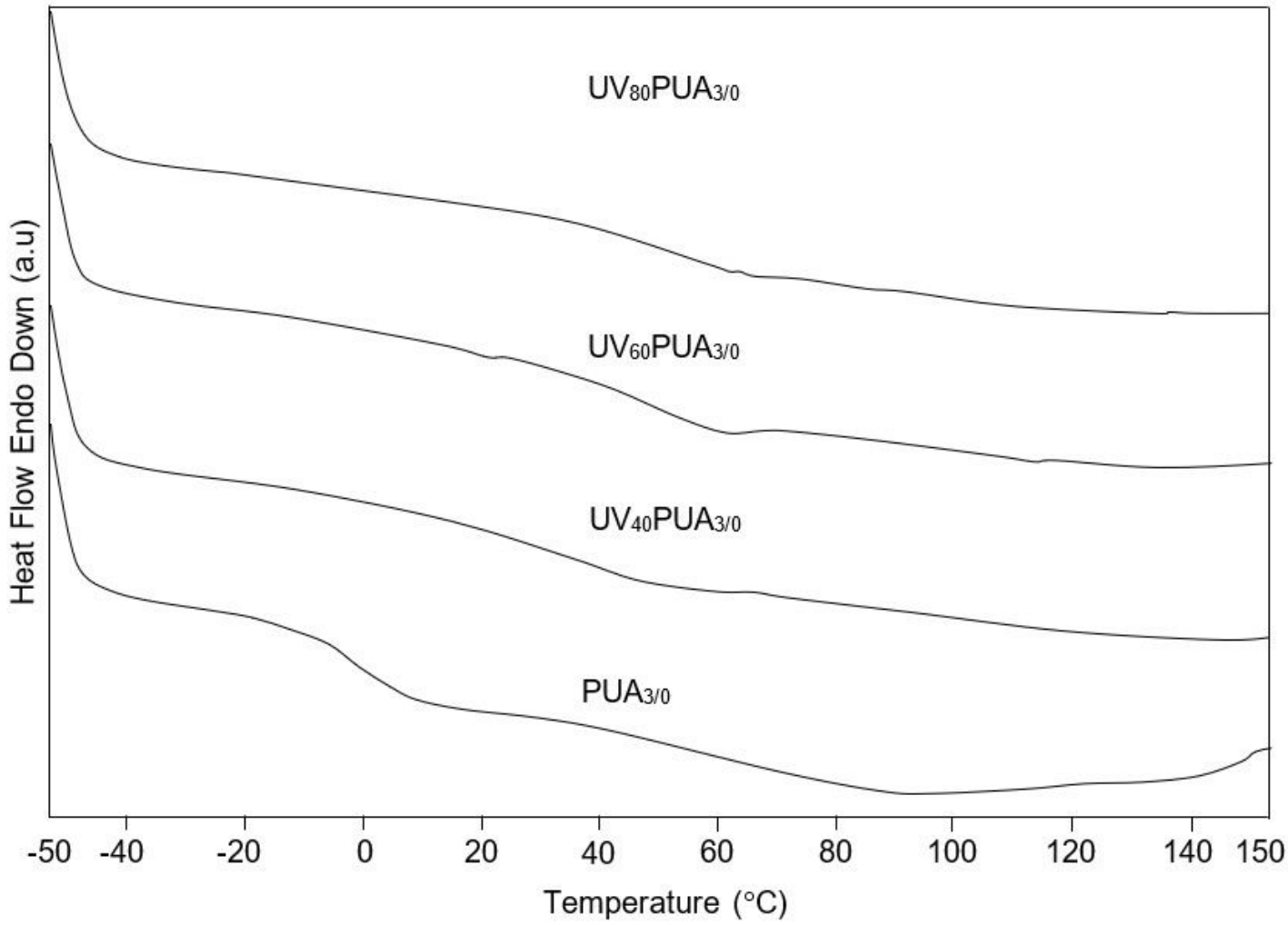

Fig. 4.

Figure 4

DSC curves of different PUA samples.

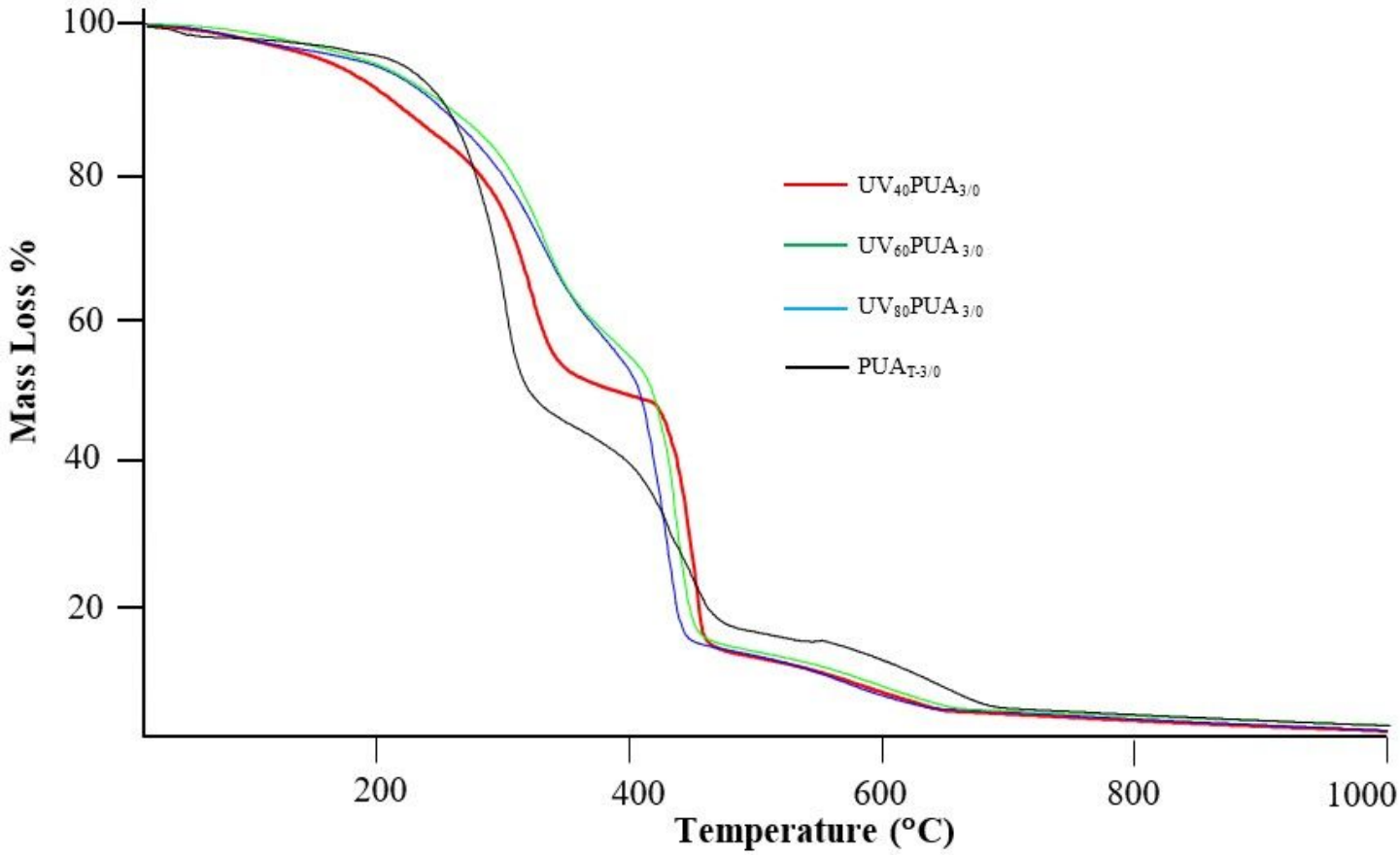

Fig. 5.

Figure 5

TG curves for studied PUA samples.

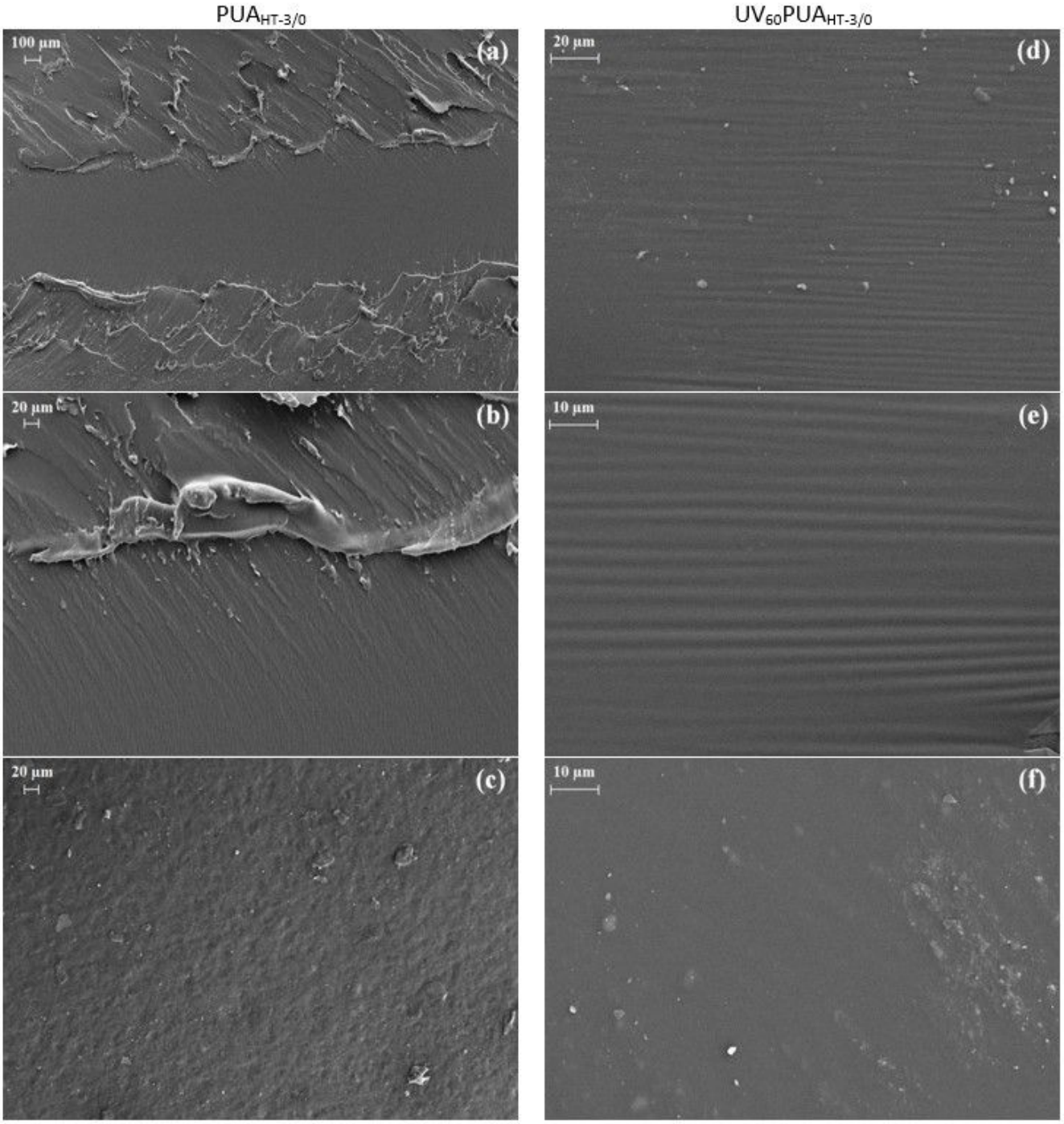

Fig. 6.

Figure 6

TG curves for studied PUA samples.